

Direct observation of homogeneous cavitation in nanopores

V. Doebele,¹ A. Benoit-Gonin,¹ F. Souris,¹ L. Cagnon,¹ P. Spathis,¹ P.E. Wolf,^{1,*}

A. Grosman,^{2,†} M. Bossert,² I. Trimaille,² C. Noûs,³ and E. Rolley^{4,‡}

¹*Université Grenoble Alpes, CNRS,*

Institut Néel, F-38042 Grenoble, France

²*Sorbonne Université, CNRS, Institut des*

NanoSciences de Paris, INSP, F-75005 Paris, France

³*Laboratoire Cogitamus 1 3/4 rue Descartes, 75005 Paris*

⁴*Laboratoire de Physique de l'Ecole Normale Supérieure,*

ENS, Université PSL, CNRS, Sorbonne Université,

Université de Paris, F-75005 Paris, France

(Dated: December 22, 2024)

Abstract

We report on the evaporation of hexane from porous alumina and silicon membranes with billions of independent nanopores tailored to an ink-bottle shape, where a cavity of diameter several tens of nanometers is separated from the bulk vapor by a constriction. For narrow enough constrictions, we demonstrate that cavity evaporation proceeds by cavitation. Measurements of the pressure dependence of the cavitation rate show that, for alumina membranes, cavitation follows the bulk, homogeneous, classical nucleation theory, definitively establishing the relevance of homogeneous cavitation as an evaporation mechanism in mesoporous materials. Our results imply that porous alumina membranes are a promising new system to study liquids in a deeply metastable state.

A porous material imbibed with a liquid can dry by two processes: recession of a liquid-vapour interface [1] or formation of vapour bubbles within the material by cavitation [2, 3]. Fundamental understanding of which of these processes is effective is crucial for many applications, ranging from characterizing porous materials [2, 3] to controlling the shrinkage of concrete [4]. In particular, this requires establishing whether cavitation occurs in the bulk of pores or on their surface, and, in the first case, whether pores are large enough for homogeneous classical cavitation theory[5] (CNT) to hold or whether confinement has to be considered [6–9].

Results from previous studies lead to contradictory conclusions. As illustrated by Fig.1, evaporation by cavitation is expected for pores presenting an ink-bottle geometry, where a wider cavity is separated from the outside vapour by a constriction narrow enough for capillarity to block the liquid-vapor interface at the cavitation pressure (Fig. 1(c)) [2, 10]. Homogeneous-like cavitation has thus been reported in materials with interconnected pores presenting cavities separated by constrictions, realizing such an ink-bottle geometry. These materials are either ordered (SBA-16 mesoporous silica [8, 10, 11], zeolites [12]) or disordered (cements [12], Vycor [13, 14], controlled porous glasses [15, 16]). In all cases, the evidence for cavitation is only indirect, relying on the interpretation of light or X-ray scattering data or, more often, on the observation of a sharp drop in the evaporation isotherm at a given pressure which is then compared to some model, usually CNT. However, in these materials, the pores have a very small diameter (several nanometers). Attractive interaction with walls should then affect the cavitation threshold, making ambiguous the identification of cavitation through comparison to CNT.

In contrast, two experiments performed on nanoporous silicon membranes with ink-bottle pores directly evidenced cavitation of nitrogen around 77 K through a two-steps shape of the evaporation isotherm, but at a much *larger* pressure than predicted by the CNT [17, 18]. This increase suggests that cavitation is heterogeneous [18], in strong contrast with the results reported for the more complex geometries above. Moreover, a similar discrepancy has been found for the cavitation of dibromomethane in Vycor [19]. These results cast a doubt on the very principle of using extensions of homogeneous CNT [2, 9] to predict the cavitation threshold in nanoporous materials.

In this paper, we elucidate this paradoxical situation by comparing evaporation of hexane from silicon and alumina membranes with pores transverse size in the range 20-60 nm,

large enough to allow a direct comparison to bulk CNT [9]. For both membranes, we directly evidence cavitation and accurately check its activated nature. Furthermore, in contrast to silicon membranes, we show that the cavitation pressure for alumina membranes is quantitatively described by bulk CNT. This definitively demonstrates the relevance of homogeneous cavitation as an evaporation mechanism in porous materials.

Our samples are fabricated using a two steps procedure [20]. We first synthesize $\simeq 1 \text{ cm}^2$ nanoporous alumina (poAl) and silicon (poSi) membranes with parallel pores, by electro-etching of highly p-doped silicon [27] or anodization of aluminum wafers [24]. In both cases, the pores, about $100 \text{ }\mu\text{m}$ long, are closed on one side of the membrane and open on the other. As illustrated in Fig. 2(a), the poAl pores are well organized with a narrow distribution in diameter around an average value of several tens of nanometers, tunable through the anodization conditions [25, 26]. We studied two alumina membranes with pore lengths $l = 57$ and $76 \text{ }\mu\text{m}$ determined by Scanning Electron Microscopy (SEM). Their respective average pore diameters were $d = 60 \text{ nm}$ and $d = 25 \text{ nm}$ determined by combining the interpore distance measured by SEM with the membrane porous volume deduced from adsorption isotherms. In contrast, the poSi pores have a polygonal cross-section (Fig. 3(c)), with a wider distribution of transverse sizes d around a mean value increasing with the sample porosity [27]. Most poSi samples have a 70% porosity corresponding to d in the range 13-40 nm ($\langle d \rangle = 26 \text{ nm}$) and l between 5 and $60 \text{ }\mu\text{m}$. In a second step, the pore aperture is reduced to obtain the desired ink-bottle geometry. For the 60 nm poAl and poSi samples, we used successive evaporations of 2 nm of aluminum followed by oxidation. For the 25 nm poAl sample, we used continuous atomic layer deposition (ALD) based on the chemical reaction between trimethylaluminum and water. SEM images show that both methods yield alumina constrictions smaller than 10 nm in diameter [28]. This upper bound is consistent with the maximal constriction diameter for observing cavitation, estimated to be 6 nm using Refs. 21–23 [20].

Condensation and evaporation of hexane in these samples were studied in optical cells, regulated at a temperature slightly below the ambient temperature, with a stability of about 1 mK. A capillary line connecting the cell to a tank of hexane at saturated vapour pressure immersed in a temperature-controlled bath is used to fill or empty the membrane through a precision microvalve at a very small flowrate. The vapour pressure P_V in the cell is measured by a pressure gauge. The amount of fluid in the pores is determined through the change Δn

of the membrane optical index measured by White Light Interferometry (WLI) [29, 30].

Figure 2 shows the successive sorption isotherms measured for the 60 nm poAl membrane as the pore aperture is progressively reduced. Here, P_V is converted to $P_L = (RT/v_L) \ln(P_V/P_{sat})$, the pressure of the liquid in equilibrium with the vapor under the assumptions of ideal gas and incompressible liquid (R is the gas constant, T the temperature and v_L the liquid molar volume). Condensation takes place at a well-defined pressure, independent of the pore aperture as expected for pores closed at one end. For the native membrane, evaporation occurs at a slightly lower pressure, probably due to some pore corrugation [31–34]. Progressively reducing the pore aperture shifts the evaporation to much lower pressures, in agreement with the expectation that evaporation is controlled by meniscus recession in constrictions (Fig. 1(b)). It also broadens the pressure range over which evaporation takes place, showing that the constrictions are distributed in diameter, either due to the initial pore diameter distribution and/or uneven deposition. The salient observation is that, for all coated samples, a sharp drop of the liquid content is observed at the *same* pressure, about -20 MPa, irrespective of the aperture reduction. The fraction of pores emptying at this pressure increases at each deposition step, and reaches nearly 100% for the last step. Since, at this stage, the constrictions necessarily remain distributed in diameter, the fact that the evaporation pressure is *sharply defined* demonstrates that evaporation takes place within the cavities, the constrictions remaining filled, in agreement with the cavitation mechanism depicted in Fig. 1(c). We stress that, in contrast to most experiments with porous materials, this evidence is direct, and does not rely on comparing the evaporation pressure value to any model.

We observe a similar behavior in poSi ink-bottles prepared in the same way as in poAl (Fig. 3(a)), also suggesting a cavitation mechanism. However, in this case, the cavitation pressure P_{cav} is much larger, around -10 MPa. Cavitation of hexane in poSi would then be heterogeneous, as previously found for nitrogen [18]. This is surprising as hexane is believed to perfectly wet most types of surfaces and should nucleate homogeneously. We thus performed complementary experiments on duplex layer poSi membranes [18]. A bottom layer with large pores – the cavities – is connected to the vapour reservoir through a top layer with narrow pores – the constrictions – (Fig. 3(c)). These constrictions are much longer than those obtained by alumina deposition, allowing WLI to *simultaneously* monitor the fluid content in the constrictions and the cavities [30]. As shown in figure 3b, cavities

empty while no evaporation is detected in the constrictions, again pointing to a cavitation mechanism [35].

When the length l and diameter d of the cavities are identical to those for the alumina-coated poSi sample ($\langle d \rangle = 26$ nm, $l = 20$ μ m), we find $P_{\text{cav}} \simeq -9.5$ MPa, close to the -10 MPa obtained in the latter case. This value depends on the cavity geometry. For fixed constrictions, we find that P_{cav} strongly depends on $\langle l \rangle$ and $\langle d \rangle$ (tuned through the porosity), ranging from -12 MPa for $\langle d \rangle = 26$ nm, $l = 4$ μ m up to -6 MPa for $\langle d \rangle = 50$ nm, $l = 20$ μ m. In a cavitation scenario, this strong dependence is not consistent with the assumption that the cavity volume (or surface in case of heterogeneous nucleation) only plays a role through the number of nucleation sites. It rather suggests that the cavity geometry impacts the energy barrier itself.

In contrast, for poAl, repeating the experiment with smaller diameter pores ($d \simeq 25$ nm) yields nearly the same value $\simeq -20$ MPa for P_{cav} although the pore volume V_p differs by a factor $\simeq 3$ between the two membranes. This observation is consistent with homogeneous cavitation, for which P_{cav} depends only weakly on the available volume. It is also consistent with the absence of confinement effect in this diameter range, as estimated from the model of Ref.9 [20].

In order to test whether cavitation in poAl is quantitatively described by CNT, we have measured its nucleation rate $\Gamma(P_L)$. A specific feature of our experimental system is that the membranes contain a very large number of *independent* pores, of the order of several $10^{10}/\text{cm}^2$. This allows us to determine the cavitation rate in a single-shot experiment, in contrast to acoustically driven [36] or thermally controlled [37] bulk cavitation experiments, where the cavitation statistics is determined over thousands of cycles. To this aim, starting from a slightly larger pressure, we quench the reservoir pressure to a stable value corresponding to P_L around -20 MPa, and monitor the temporal decay of the number of filled pores by measuring the light transmission through the membrane. The totally empty or filled membrane is nearly homogeneous on the scale of the light wavelength and scatters little. In contrast, when stochastic cavitation takes place, the pores randomly empty, giving rise to local fluctuations of the refractive index and strong light scattering, resulting in a reduced transmission. This effect can be directly evidenced by illuminating the membrane with a wide collimated light beam and precisely quantified by measuring the transmission of a laser beam [20].

We have performed such experiments for the two alumina membranes. As expected for a stochastic process, the number of filled pores decreases exponentially with time with a time constant τ (Inset of Fig. 4 for the 60 nm membrane). Repeating this quench at different depths yields $\tau(P_L)$, from which we deduce the cavitation rate per unit time and unit volume $\Gamma(P_L) = (V_p \tau(P_L))^{-1}$.

Figure 4 shows that $\Gamma(P_L)$ increases by nearly 3 orders of magnitude when changing P_V , hence P_L , by only 5%. This large increase exemplifies the exponential dependence of the relaxation time on the energy barrier. Using a slightly different method, we find a similar behavior for silicon membranes, also showing the activated nature of the evaporation process in this case [20].

To our knowledge, these results are the first evidence for the stochastic and activated nature of cavitation in nanoporous materials. The relaxation rate can be compared to the CNT prediction [5] $\Gamma = \Gamma_0 \exp(-E_b/k_B T)$, where Γ_0 is an attempt rate and the energy barrier E_b is given by:

$$E_b = \frac{16\pi\sigma^3}{3(P_V - P_L)^2} \quad (1)$$

where σ is the surface tension. Different expressions for Γ_0 [5, 38] lead to $\Gamma_0 = 2.10^{38} \text{ m}^{-3} \text{ s}^{-1}$ within a factor of 10. As shown by Fig.4, using this value and the bulk surface tension (0.185 J/m² at 19°C [39]) leads to predicted rates about 10^7 too small over the full pressure range, corresponding to a predicted cavitation pressure 15% larger than observed. Keeping $\Gamma_0 = 2.10^{38} \text{ m}^{-3} \text{ s}^{-1}$, an approximate agreement with experiments requires to reduce the surface tension σ by about 9% with respect to its bulk value. A similar difference has been measured in the case of bulk cavitation of heptane and ascribed to a reduction of the surface tension due the large curvature of the critical germ [40]. However, adjusting only Γ_0 or σ does not allow to match the experimental Γ vs P_L data over the full pressure range. Such a match requires to combine a 5% reduction of σ *with* an increase of Γ_0 by a factor $\simeq 500$. This might point to the fact that the above expressions of the CNT attempt rate are underestimated.

To summarize, we show that cavitation of hexane in porous alumina ink-bottles with cavity diameters of several tens of nanometers closely follows the predictions of the bulk homogeneous classical nucleation theory. This confirms that homogeneous cavitation is a relevant mechanism in nanoporous systems, as assumed by previous studies on materials with interconnected pores. This opens the way to performing similar experiments with

pores of smaller diameter (below 10 nm) in order to quantitatively test extensions of CNT in presence of confinement. In contrast, we confirm that porous silicon ink-bottles exhibit heterogeneous cavitation. More studies will be required to understand whether this is specific to the particular structure of poSi.

Finally, our work opens new prospects for fundamental studies of cavitation. In contrast to cavitation acoustically driven at MHz frequencies, our experiments are essentially static, allowing to precisely measure the relaxation rate at a given pressure. Also, in contrast to the so-called artificial-tree technique [41], where cavitation is probed in macroscopic cavities closed by a single porous layer, nanoporous membranes with independent nanopores tolerate the existence of a small density of leaky constrictions. PoAl membranes are thus a promising system to address points of current debate, such as the influence of superfluidity of liquid helium on its cavitation [42], or the origin of the too large cavitation pressure observed for water in the artificial-tree geometry [43]. Beyond these examples, by allowing to decrease the liquid pressure down to its tensile limit, these membranes open a new route to study liquids in deeply metastable states.

This paper is dedicated to the memory of our late co-author and colleague A. Grosman. We thank K. Davitt for her critical reading. We acknowledge the financial support of Agence Nationale de la Recherche through the project CavConf, ANR-17-CE30-0002, including the funding of F. S. and M. B., and of Université Grenoble Alpes which funded V.D. through an AGIR PhD grant.

* pierre-etienne.wolf@neel.cnrs.fr

† deceased, 2019 August 29th

‡ rolley@phys.ens.fr

- [1] Mason G. Determination of the pore-size distributions and pore-space interconnectivity of Vycor porous glass from adsorption-desorption hysteresis capillary condensation isotherms. *Proc. R. Soc. Lond.*, **415**, 453 (1988).
- [2] Ravikovitch P and Neimark A. Experimental confirmation of different mechanisms of evaporation from ink-bottle type pores: Equilibrium, pore blocking, and cavitation. *Langmuir*, **18**, 9830 (2002).

- [3] Monson P. Understanding adsorption/desorption hysteresis for fluids in mesoporous materials using simple molecular models and classical density functional theory. *Micropor. Mesopor. Mat.*, **160**, 47 (2012).
- [4] Maruyama I, Gartner E, Beppu K, and Kurihara R. Role of alcohol-ethylene oxide polymers on the reduction of shrinkage of cement paste. *Cement and Concrete Research*, **111**, 157 (2018).
- [5] Blander M and Katz J. Bubble nucleation in liquids. *AIChE Journal*, **21** (1975).
- [6] Vishnyakov A and Neimark A. Monte Carlo simulation test of pore blocking effects. *Langmuir*, **19**, 3240 (2003).
- [7] Vishnyakov A and Neimark A. Nucleation of liquid bridges and bubbles in nanoscale capillaries. *J. Chem. Phys.*, **119**, 9755 (2003).
- [8] Rasmussen C J, Vishnyakov A, Thommes M, Smarsly B M, Kleitz F, and Neimark A V. Cavitation in Metastable Liquid Nitrogen Confined to Nanoscale Pores. *Langmuir*, **26**, 10147 (2010).
- [9] Bonnet F and Wolf P E. Thermally activated condensation and evaporation in cylindrical pores. *J. Phys. Chem. C*, **123**, 1335 (2019).
- [10] Morishige K and Tateishi N. Adsorption hysteresis in ink-bottle pore. *J. Chem. Phys.*, **119**, 2301 (2003).
- [11] Morishige K, Tateishi M, Hirose F, and Aramaki K. Change in desorption mechanism from pore blocking to cavitation with temperature for nitrogen in ordered silica with cagelike pores. *Langmuir*, **22**, 9220 (2006).
- [12] Maruyama I, Rymeš J, Vandamme M, and Coasne B. Cavitation of water in hardened cement paste under short-term desorption measurements. *Materials and Structures*, **51**, 159 (2018).
- [13] Morishige K. Hysteresis Critical Point of Nitrogen in Porous Glass: Occurrence of Sample Spanning Transition in Capillary Condensation. *Langmuir*, **25**, 6221 (2009).
- [14] Bonnet F, Melich M, Puech L, Anglès d'Auriac J C, and Wolf P E. On condensation and evaporation mechanisms in disordered porous materials. *Langmuir*, **35**, 5140 (2019).
- [15] Machin W D. Properties of three capillary fluids in critical region. *Langmuir*, **15**, 169 (1999).
- [16] Reichenbach C, Kalies G, Enke D, and Klank D. Cavitation and pore blocking in nanoporous glasses. *Langmuir*, **27**, 10699 (2011).
- [17] Wallacher D, Kunzner N, Kovalev D, Knorr N, and Knorr K. Capillary condensation in linear

- mesopores of different shape. *Phys. Rev. Lett.*, **92**, 195704 (2004).
- [18] Grosman A and Ortega C. Cavitation in Metastable Fluids Confined to Linear Mesopores. *Langmuir*, **27**, 2364 (2011).
 - [19] Mitropoulos A C, Stefanopoulos K L, Favvas E P, Vansant E, and Hankins N P. On the formation of nanobubbles in Vycor porous glass during the desorption of halogenated hydrocarbons. *Scientific Reports*, **5**, 10943 (2015).
 - [20] See Supplemental Material at [URL will be inserted by publisher] for details on the sample preparation, the measurements methods, and the analysis of the results.
 - [21] Saam W F and Cole M W. Excitations and thermodynamics for liquid-helium films. *Phys. Rev. B*, **11**, 1086 (1975).
 - [22] Israelachvili J N. Intermolecular and Surface Forces (Third Edition), (Academic Press, San Diego 2011).
 - [23] Van Oss C J, Chaudhury M K, and Good R J. Interfacial Lifshitz-Van der Waals and polar interactions in macroscopic systems. *Chem. Rev.*, **88**, 927 (1988).
 - [24] Masuda H and Fukuda K. Ordered metal nanohole arrays made by a two-step replication of honeycomb structures of anodic alumina. *Science*, **268**, 1466 (1995).
 - [25] Lee W, Schwirn K, Steinhart M, Pippel E, Scholz R, and Gosele U. Structural engineering of nanoporous anodic aluminium oxide by pulse anodization of aluminium. *Nat. Nano*, **3**, 234 (2008).
 - [26] Lee W and Park S J. Porous anodic aluminum oxide: Anodization and templated synthesis of functional nanostructures. *Chem. Rev.*, **114**, 7487 (2014).
 - [27] Grosman A and Ortega C. Capillary condensation in porous materials. hysteresis and interaction mechanism without pore blocking/percolation process. *Langmuir*, **24**, 3977 (2008).
 - [28] This is smaller than for previous experiments performed on alumina membranes with ink-bottle pores, reported in Refs.[30, 32], explaining why cavitation has not been observed in these experiments.
 - [29] Pacholski C, Sartor M, Sailor M J, Cunin F, and Miskelly G M. Biosensing using porous silicon double-layer interferometers: Reflective interferometric Fourier transform spectroscopy. *J. Am. Chem. Soc.*, **127**, 11636 (2005).
 - [30] Casanova F, Chiang C E, Li C P, and Schuller I K. Direct observation of cooperative effects in capillary condensation: The hysteretic origin. *Appl. Phys. Lett.*, **91**, 243103 (2007).

- [31] Puibasset J. Adsorption/desorption hysteresis of simple fluids confined in realistic heterogeneous silica mesopores of micrometric length: A new analysis exploiting a multiscale Monte Carlo approach. *J. Chem. Phys.*, **127**, 154701 (2007).
- [32] Bruschi L, Mistura G, Nguyen P T M, Do D D, Nicholson D, Park S J, and Lee W. Adsorption in alumina pores open at one and at both ends. *Nanoscale*, **7**, 2587 (2015).
- [33] Morishige K. Nature of adsorption hysteresis in cylindrical pores: Effect of pore corrugation. *J. Phys. Chem. C*, **120**, 22508 (2016).
- [34] Doebele V. Condensation et évaporation de l’hexane dans les membranes d’alumine poreuse. Ph.D. thesis, Université Grenoble-Alpes (2019).
- [35] An alternative scenario could be that the pores of poSi communicate, and empty through a very small number of large enough constrictions.
- [36] Pettersen M S, Balibar S, and Maris H J. Experimental investigation of cavitation in superfluid ^4He . *Phys. Rev. B*, **49**, 12062 (1994).
- [37] Azouzi M E M, Ramboz C, Lenain J F, and Caupin F. A coherent picture of water at extreme negative pressure. *Nat. Phys.*, **9**, 38 (2013).
- [38] Maris H J and Xiong Q. Nucleation of bubbles in liquid helium at negative pressure. *Phys. Rev. Lett.*, **63**, 1078 (1989).
- [39] Lemmon E. W., McLinden M. O. and Friend D. G., "Thermophysical Properties of Fluid Systems" in WebBook of Chemistry NIST, NIST Standard Reference Database SRD Number 69, Eds. P.J. Linstrom and W.G. Mallard, National Institute of Standards and Technology, Gaithersburg MD, 20899, <https://doi.org/10.18434/T4D303>, (downloaded April 10th, 2020).
- [40] Bruot N and Caupin F. Curvature dependence of the liquid-vapor surface tension beyond the Tolman approximation. *Phys. Rev. Lett.*, **116**, 056102 (2016).
- [41] Wheeler T D and Stroock A D. The transpiration of water at negative pressures in a synthetic tree. *Nature*, **455**, 208 (2008).
- [42] Qu A, Trimeche A, Dupont-Roc J, Grucker J, and Jacquier P. Cavitation density of superfluid helium-4 around 1 K. *Phys. Rev. B*, **91**, 214115 (2015).
- [43] Caupin F, Arvengas A, Davitt K, Azouzi M E M, Shmulovich K I, Ramboz C, Sessoms D A, and Stroock A D. Exploring water and other liquids at negative pressure. *J. Phys. Cond. Mat.*, **24** (2012).

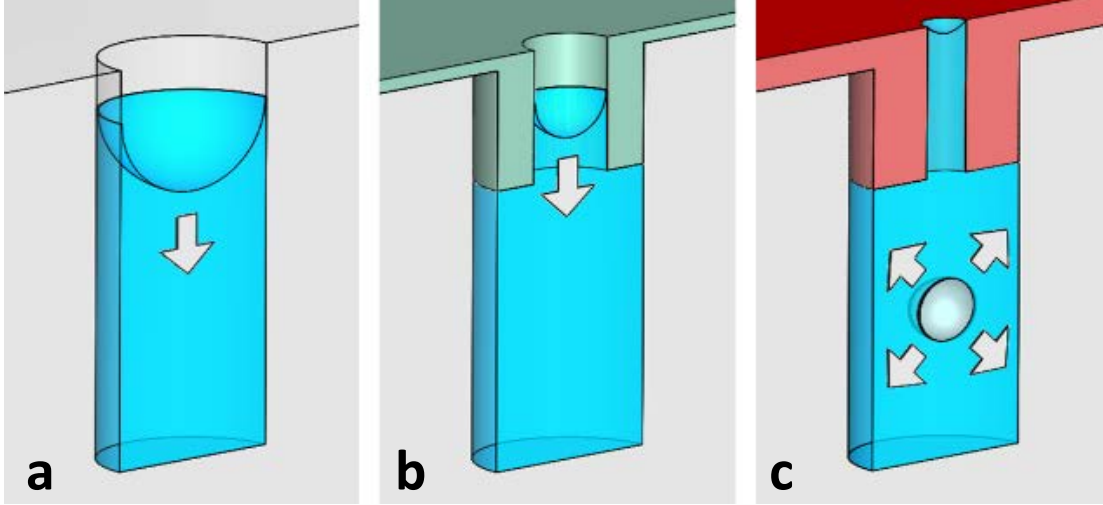


FIG. 1. Cavitation in an ink-bottle geometry. **(a)** A straight cylindrical pore opened to a vapour reservoir empties through recession of the liquid-vapour meniscus. The smaller the pore diameter, the smaller the evaporation pressure. **(b,c)** Two possible evaporation mechanisms for a cavity ended by a cylindrical constriction; **(b)** The constriction empties at its equilibrium pressure, triggering further evaporation in the wider cavity through meniscus recession; **(c)** If the constriction is narrow enough for its evaporation pressure to lie below the cavitation threshold, the cavity empties by cavitation, while the constriction remains filled with liquid.

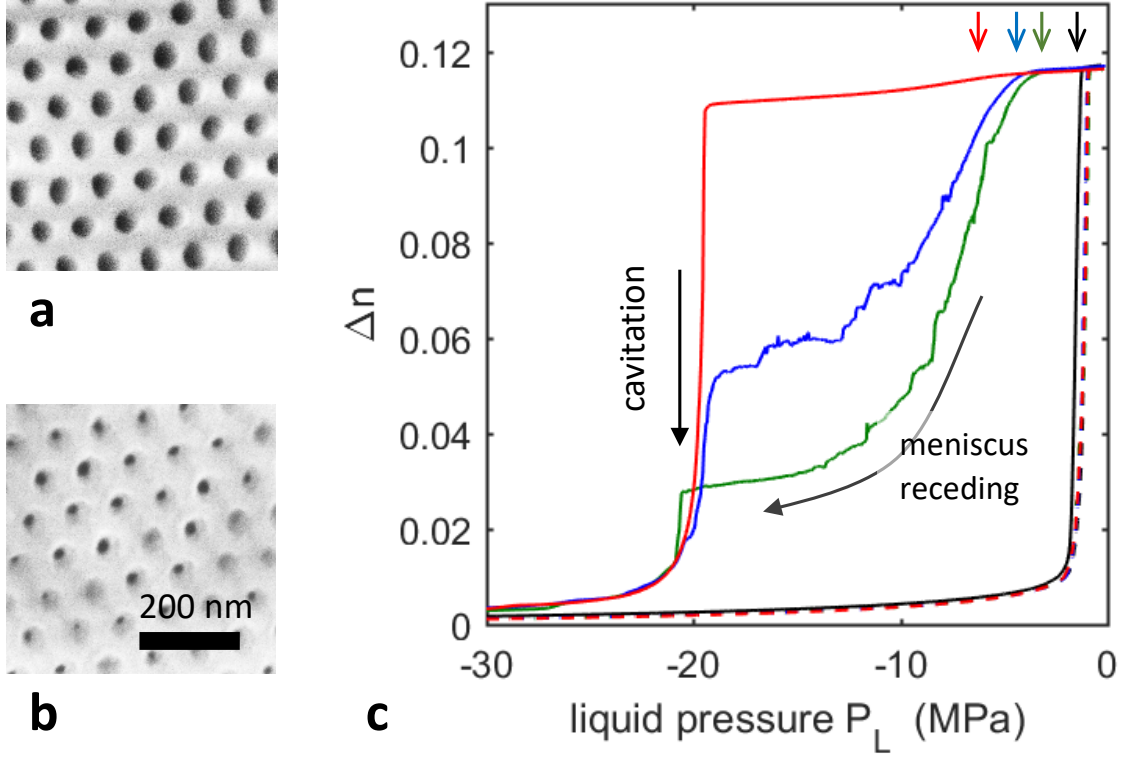


FIG. 2. (color online) Cavitation in an alumina membrane. Starting from a native alumina membrane with 60 nm diameter pores (a), successive 2 nm thick alumina layers are deposited at the mouth of the pore, reducing the pore aperture (b: 8 layers). Sorption isotherms of hexane are measured at 18°C (c) as described in the text. The membrane fluid content is deduced from Δn , the change of the membrane optical index with respect to the empty state. The (superimposed) dashed curves are the condensation isotherms, and the continuous lines the evaporation isotherms, for increasing deposits of alumina at the pore mouth (black : native; green: 8 layers; blue: 10 layers; red: 12 layers). For intermediate coatings, the noise is due to a loss of contrast of the interference pattern (resulting from a strong light scattering [20]). The sharp drop at -20 MPa is the signature of cavitation.

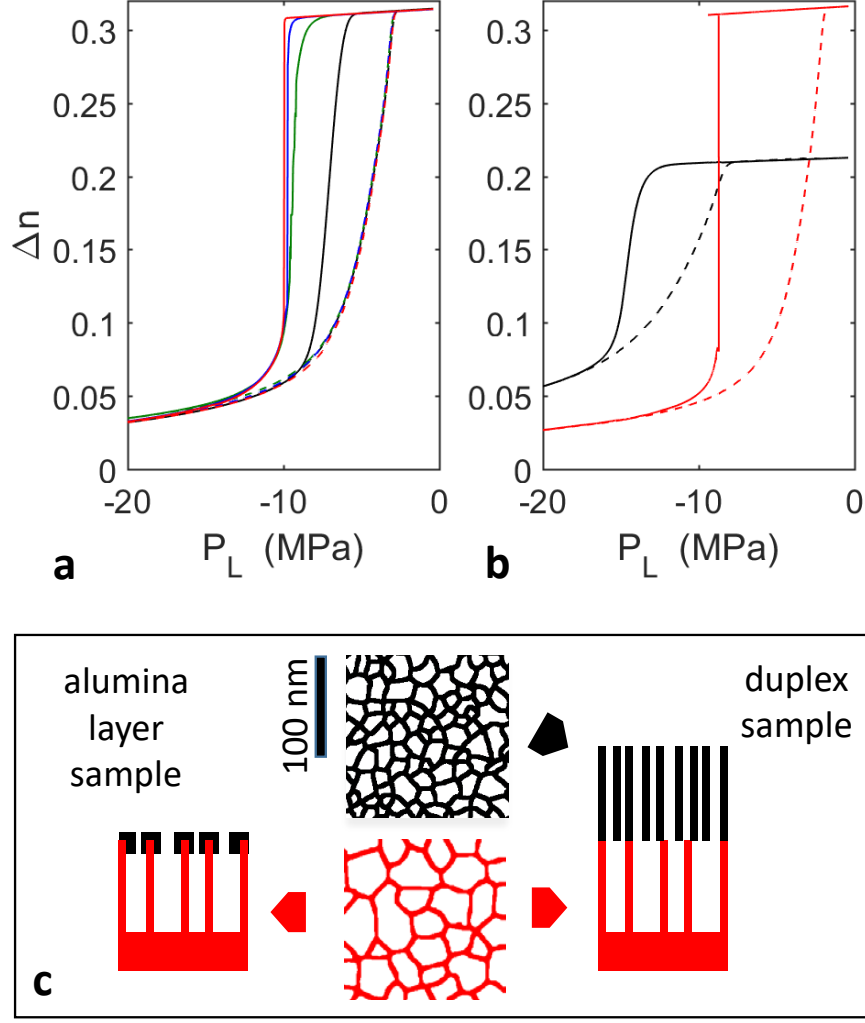


FIG. 3. (color online) Cavitation in porous silicon ink-bottles: (a) isotherms for an alumina-coated poSi sample (left part of box c). Dashed lines correspond to condensation and full lines to evaporation. Black: poSi as prepared ($\langle d \rangle = 26$ nm, pore length $l = 20 \mu\text{m}$). Green/Blue/Red: poSi coated by 2/6/8 alumina layers. For as-prepared poSi, the condensation isotherm is much less steep than in the case of poAl, reflecting the wider distribution of pore diameters. (b) isotherms obtained on a duplex layer sample formed by successively electro-etching a top layer with small pores $\langle d \rangle = 12$ nm and a bottom layer with small pores $\langle d \rangle = 26$ nm (right part of box c). The contributions of the two layers are plotted separately in black for the bottom layer and in red/grey for the top layer. (c) binarized Transmission Electron Microscopy (TEM) images of the cross-section of cavities ($\langle d \rangle = 26$ nm, black) and of the constrictions of the duplex sample ($\langle d \rangle = 12$ nm, red/grey).

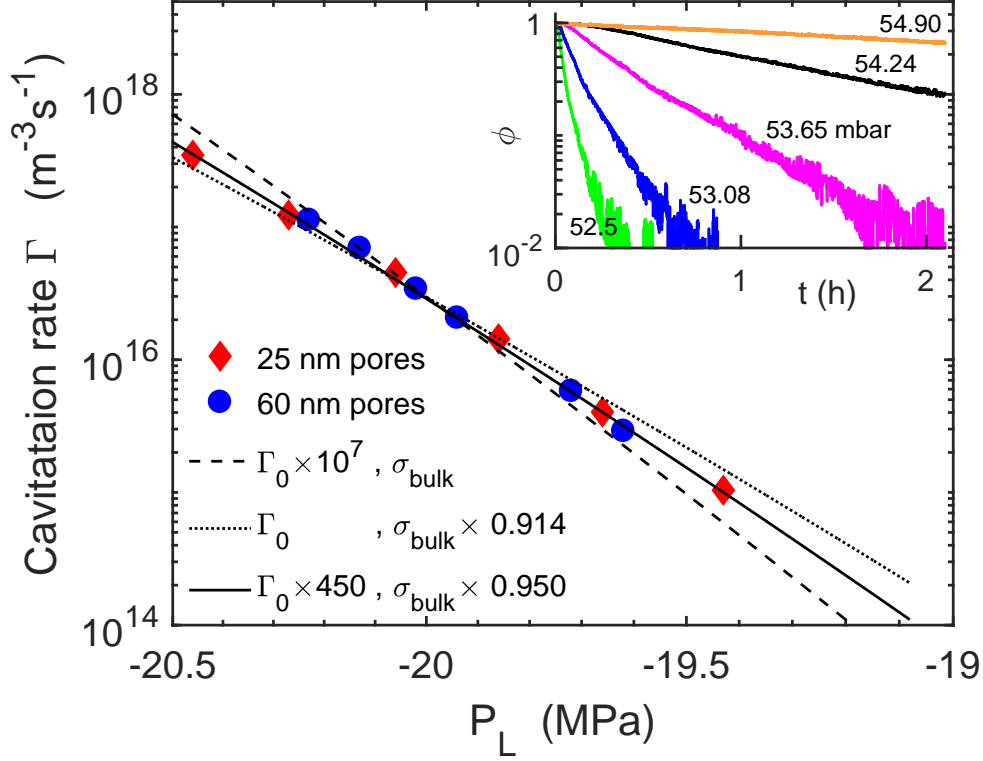


FIG. 4. Cavitation rate Γ at 19°C as a function of liquid pressure P_L for poAl membranes with average pore diameters $d = 60$ nm and $d = 25$ nm. Γ is measured from the exponential decay of the number of filled pores following a quench of the pressure reservoir from 60 mb down to a lower pressure ranging between 52 and 55 mbar, as illustrated in the inset for the 60 nm membrane. The fraction of filled pores ϕ is measured through the logarithm of the optical transmission and normalized to its value at time $t=0$, corresponding to a 10% transmission [20]. The cavitation rate per unit volume Γ is deduced by dividing the decay rate by the pore volume, computed using $d = 56$ nm and $d = 27$ nm. These values lie within the error bars of the measured above values, and are such that $\Gamma(P_L)$ is identical for the two membranes. Lines correspond to the CNT predictions for different values of the attempt rate or the surface tension (see text).